THESIS FOR THE DEGREE OF LICENTIATE OF ENGINEERING IN SOLID AND STRUCTURAL MECHANICS

On computational homogenization of fracturing continua

ERIK SVENNING

Department of Applied Mechanics
CHALMERS UNIVERSITY OF TECHNOLOGY
Gothenburg, Sweden 2015

On computational homogenization of fracturing continua
ERIK SVENNING

Thesis for the degree of Licentiate of Engineering 2015:10
ISSN 1652-8565
Department of Applied Mechanics
Chalmers University of Technology
SE-412 96 Gothenburg
Sweden
Telephone: +46 (0)31-772 1000

Cover:
A Statistical Volume Element (SVE) in a material containing cracks (left) and simulated deformation of the SVE (right).

Chalmers Reproservice
Gothenburg, Sweden 2015

On computational homogenization of fracturing continua
Thesis for the degree of Licentiate of Engineering in Solid and Structural Mechanics
ERIK SVENNING
Department of Applied Mechanics
Chalmers University of Technology

Abstract

Ductile fracture is important to control in many industrial processes, be it a desired phenomenon (e.g. in metal cutting) or a failure to be prevented (e.g. in structures subject to blast loading). Increased understanding of the fracture processes can be gained by using computational homogenization, where the nucleation and growth of microscopic cracks is explicitly modeled and included in the effective response of a Statistical Volume Element (SVE)[1]. Choosing suitable boundary conditions on the SVE is challenging, because conventional boundary conditions (Dirichlet, Neumann and strong periodic) are inaccurate when cracks are present in the SVE. In the present work, we instead impose periodic boundary conditions in a weak sense on the SVE, leading to a mixed variational format with displacements and boundary tractions as unknowns. By constructing a suitable traction approximation, the boundary conditions can be adapted to the problem at hand in order to gain improved convergence. To this end, we propose a stable traction approximation that is piecewise constant between crack-boundary intersections and we show analytically that the LBB (inf-sup) condition is fulfilled for the proposed approximation.

The weakly periodic boundary conditions are combined with the eXtended Finite Element Method (XFEM), cohesive zones and the concept of material forces to perform numerical simulations of materials undergoing crack propagation on the microscale. The numerical examples show that weakly periodic boundary conditions with a suitably chosen traction approximation are more efficient than conventional boundary conditions in terms of convergence with increasing SVE size. This observation holds for stationary cracks as well as for propagating cracks.

The work presented in this thesis is concerned with homogenization of damage evolution prior to localization, which is a prerequisite for accurate multiscale modeling of localization.

Keywords: XFEM, Computational Homogenization, Weak periodicity, Crack propagation

[1] Sometimes also called Representative Volume Element (RVE).

Till Annie och Ida.

Preface

The work presented in this thesis has been carried out from May 2013 to May 2015 at the Division of Material and Computational Mechanics at Chalmers University of Technology. The research was financially supported by the Swedish Research Council (Vetenskapsrådet) under contract 2012-3006.

I would like to thank my supervisors Professor Fredrik Larsson and Assistant Professor Martin Fagerström for their guidance and encouragement. I would also like to thank my colleagues for the nice working environment and for many interesting discussions. Finally, I would like to thank my family for their love and support.

Gothenburg, April 2015
Erik Svenning

Thesis

This thesis consists of an extended summary and the following appended papers:

Paper A E. Svenning, M. Fagerström and F. Larsson. Computational homogenization of microfractured continua using weakly periodic boundary conditions. *Submitted for international publication.*

Paper B E. Svenning, M. Fagerström and F. Larsson. Computational homogenization of microstructures undergoing crack propagation. *To be submitted.*

The appended papers were prepared in collaboration with the co-authors. The author of this thesis was responsible for the major progress of the work, i.e. took part in planning the papers, took part in developing the theory, developed the numerical implementation, carried out numerical simulations and wrote the papers.

Contents

Part I
Extended Summary

1 Introduction

Ductile fracture of metals is relevant in many engineering applications, be it a desired phenomenon as e.g. in metal cutting or a failure to be prevented as e.g. in structures subject to blast loading. The importance of damage and fracture phenomena has lead to the development of a wide range of modeling approaches [1, 2], ranging from local and nonlocal continuum damage models to discrete crack models represented by cohesive zones, embedded discontinuities and the eXtended Finite Element Method (XFEM). Within the framework of discrete crack models, several authors have explored the possibilities of combining element embedded discontinuities or XFEM with fracture criteria based on stress intensity factors [3, 4], material crack driving force [5], stress [6, 7], plastic strain [8] or loss of ellipticity [9].

However, since fracture starts with the nucleation of microscopic cracks that grow and eventually evolve into macroscopic cracks, it is natural to seek increased knowledge by studying the nucleation and growth of cracks on the microscale, see e.g. [10] in the context of crystal plasticity. A suitable tool to connect the scales is computational homogenization that can be used to determine the effective response of a material sample containing growing cracks. The growth of microcracks into macrocracks is typically modeled by injecting a macroscopic discontinuity into the model when some localization criterion is fulfilled [11], whereby the failure can be represented by means of cohesive zone elements [12], XFEM [13, 14] or embedded discontinuities [15, 16].

Note, however, that an accurate model of microscale damage progression is a prerequisite for accurate localization models. Hence, the topic of this thesis is how to properly set up the microscale model, including suitable boundary conditions and crack growth models. Critical steps in this task are to establish a finite element formulation of the governing equations including a suitable representation of propagating cracks as discussed in Chapter 3 and to establish a multiscale model of the problem as discussed in Chapter 4.

2 Aim of research

The long term goal of the present work is to develop techniques for multiscale modeling of ductile fracture in metals. This goal involves the following challenges:

1. Develop suitable boundary conditions on the Statistical Volume Element (SVE) and investigate how the effective response depends on the SVE size.

2. Develop accurate microscale models that take the damage progression on the microscale into account.

3. Develop multiscale modeling techniques capable of handling localization on the microscale as well as on the macroscale.

4. Use the multiscale modeling framework to develop accurate and efficient phenomenological models.

Challenge 1 and, partly, challenge 2 are addressed in this thesis, while challenges 3 and 4 are left as future work.

3 A model of a fracturing continuum

3.1 Preliminaries

To establish a suitable finite element formulation for a body containing propagating cracks, we consider a specimen occupying the domain Ω with boundary Γ_{ext} as shown in Figure 3.1. Cracks in the specimen are explicitly modeled as internal boundaries Γ_{int} (in contrast to using an implicit representation in terms of e.g. a smeared crack model). To be specific, Γ_{int} is a two-sided surface with a positive side Γ_{int}^+ and a negative side Γ_{int}^-. Letting superscripts $^+$ and $^-$ denote quantities on Γ_{int}^+ and Γ_{int}^-, respectively, we define the normal $\boldsymbol{n}_{int}$ to be the outward unit normal on Γ_{int}^-, i.e. $\boldsymbol{n}_{int} \stackrel{\text{def}}{=} \boldsymbol{n}_{int}^-$. For future use, we also define the jump of a quantity over Γ_{int}^+ as $[\![\boldsymbol{u}]\!] \stackrel{\text{def}}{=} \boldsymbol{u}^+ - \boldsymbol{u}^-$.

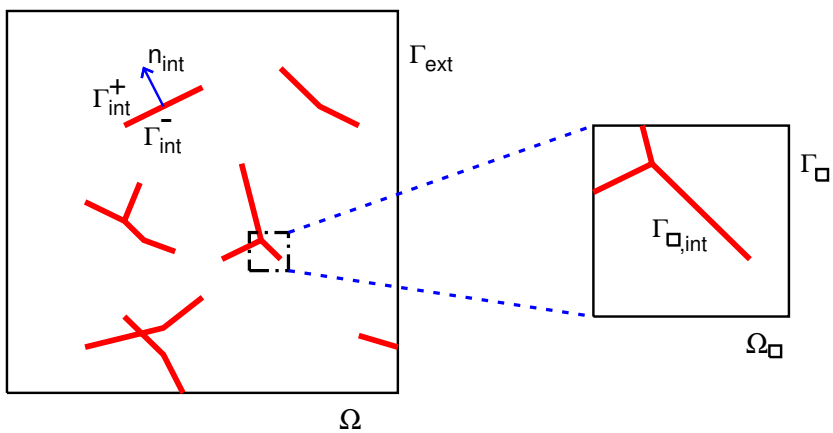

Figure 3.1: *Domain Ω with external boundary Γ_{ext} and internal boundaries Γ_{int}. A Statistical Volume Element (SVE) with domain $\Omega_\square$ and boundary $\Gamma_\square$ is also shown.*

To proceed, we assume quasistatic loading and small strains. Neglecting the body

force, the strong form of the equilibrium equations are then written in standard fashion as

$$\begin{aligned} -\boldsymbol{\sigma}\cdot\boldsymbol{\nabla} &= \mathbf{0} \text{ in } \Omega, \\ \boldsymbol{t}^+ + \boldsymbol{t}^- &= \mathbf{0} \text{ on } \Gamma_{int}, \\ \boldsymbol{t} &= \hat{\boldsymbol{t}} \text{ on } \Gamma_{ext,N}, \\ \boldsymbol{u} &= \hat{\boldsymbol{u}} \text{ on } \Gamma_{ext,D}, \end{aligned} \tag{3.1}$$

where $\boldsymbol{\sigma} = \boldsymbol{\sigma}([\boldsymbol{u}\otimes\boldsymbol{\nabla}]^{sym})$ is the Cauchy stress, $\boldsymbol{\nabla}$ is the gradient operator, $\hat{\boldsymbol{t}}$ is a prescribed traction and $\hat{\boldsymbol{u}}$ is a prescribed displacement. The traction on the internal boundaries, which is linked to the continuum stress by $\boldsymbol{t}^+ = -\boldsymbol{\sigma}|_{\Gamma^+_{int}}\cdot\boldsymbol{n}_{int}$ and $\boldsymbol{t}^- = \boldsymbol{\sigma}|_{\Gamma^-_{int}}\cdot\boldsymbol{n}_{int}$, may be described by a cohesive zone law specifying $\boldsymbol{t} \overset{\text{def}}{=} \boldsymbol{t}^+ = -\boldsymbol{t}^-$ in terms of the jump $[\![\boldsymbol{u}]\!]$ over the crack faces.

The weak solution corresponding to Equation (3.1) is obtained by finding $\boldsymbol{u}\in\mathbb{U}$ such that

$$\begin{aligned} \int_\Omega \boldsymbol{\sigma} : [\delta\boldsymbol{u}\otimes\boldsymbol{\nabla}]\,\mathrm{d}\Omega - \int_{\Gamma^+_{int}} \boldsymbol{t}\cdot[\![\delta\boldsymbol{u}]\!]\,\mathrm{d}\Gamma &= \int_{\Gamma_{ext,N}} \hat{\boldsymbol{t}}\cdot\delta\boldsymbol{u}\,\mathrm{d}\Gamma \;\forall\delta\boldsymbol{u}\in\mathbb{U}^0, \\ \mathbb{U} &= \left\{\boldsymbol{v} : \boldsymbol{v}\in\left[\mathbb{H}^1(\Omega)\right]^d,\ \boldsymbol{v}=\hat{\boldsymbol{u}} \text{ on } \Gamma_{ext,D}\right\}, \\ \mathbb{U}^0 &= \left\{\boldsymbol{v} : \boldsymbol{v}\in\left[\mathbb{H}^1(\Omega)\right]^d,\ \boldsymbol{v}=\mathbf{0} \text{ on } \Gamma_{ext,D}\right\}, \end{aligned} \tag{3.2}$$

where $\mathbb{H}^1(\Omega)$ denotes the Sobolev space of functions with square integrable gradients on Ω and d denotes the dimension of the problem. We note that $\boldsymbol{u}$ and $\delta\boldsymbol{u}$ do not need to be continuous across Γ_{int}. More precisely, the internal boundaries Γ_{int} represent cracks that will be modeled using the XFEM as discussed below.

3.2 The eXtended Finite Element Method (XFEM)

The eXtended Finite Element Method (XFEM) is suitable for modeling of crack propagation since it allows a kinematic crack representation that is independent of the underlying finite element mesh. The XFEM has been frequently used to model crack propagation since the classical work by Belytschko and Black [17], and has today reached a quite high level of maturity, with applications to a wide range of engineering problems [18]. Nevertheless, several challenges need to be addressed in order to successfully apply XFEM to crack propagation problems.

Since the purpose of applying XFEM is to avoid meshing cracks explicitly, a separate representation of the crack geometry is needed. Alternatives are to use the level set method, or to represent the crack explicitly using for example a polygon. In the present work, a hybrid representation is used, where a polygon representation is used to compute the necessary level set fields [19]. Furthermore, if branching or intersecting cracks are considered, it is not sufficient to add enrichments for each crack separately. The crack intersections need special treatment, e.g. by using so called *junction functions* [20].

Regarding accuracy, we remark that using a pure step enrichment gives poor accuracy in the predicted stress field if the mesh is not extremely fine, especially for elastic problems.

Much better accuracy can be obtained by enriching with asymptotic functions close to crack tips as first suggested in [21]. To allow straightforward enforcement of boundary conditions, a shifted enrichment can be used in order to preserve the Kronecker-δ property of the discretization [22].

Regarding numerical issues, it should also be noted that ill-conditioning occurs if a crack passes very close to, or exactly in, a node. Possible remedies are, among others, to simply disallow cracks too close to nodes or to add numerical stabilization based on an eigenvalue analysis of the stiffness matrix [23].

In the present work, we consider XFEM based on the partition of unity concept [24, 17] and use a hybrid geometry representation as stated above. Crack intersections are handled using *junction functions* [20]. A shifted enrichment is employed to preserve the Kronecker-δ property and elements containing a crack tip are enriched with asymptotic functions.

The XFEM as described above provides a kinematic representation of cracks in the material. It can be combined with cohesive zone models describing the constitutive behavior at the crack faces as well as models for crack propagation as described below.

3.3 Cohesive zone models

The cohesive zone concept [25, 26], which can be used in combination with XFEM [27, 4] as well as with interface elements [28], allows modeling of ductile fracture by describing the crack surface traction in terms of the displacement jump over the crack. The most common approach is to use a pure displacement based formulation, where the traction is computed directly from the traction discontinuity on the integration point level. Alternatives are to introduce additional unknowns for the traction, leading to a mixed formulation [29, 30], or to combine cohesive zones with Nitsche's method [31]. A formulation with only displacements as unknowns has the obvious advantages of easy implementation and fewer unknowns in the global system of equations. A serious drawback is that the use of a high penalty stiffness may lead to ill-conditioning as well as spurious oscillations in the traction field [32] (see also [33] in the context of contact).

We remark that the problem of formulating a cohesive zone model describing the interface traction $\boldsymbol{t}$ in terms of the interface displacement discontinuity $[\![\boldsymbol{u}]\!]$ has been the subject of many investigations. Here, we are not concerned with the formulation of new cohesive zone models, but we will use a damage-plasticity model based on the developments in [34] in some of the numerical examples. Furthermore, we will use a linear elastic cohesive zone model with low penalty stiffness as regularization in some examples.

3.4 Crack propagation models

Crack growth can be modeled by combining the XFEM with criteria for the onset and direction of crack growth. Without attempting to list all developments in the field, we first note that models describing crack propagation are not fundamentally tied to the chosen crack representation. For example, crack propagation based on stress intensity factors was studied by Zi and Belytschko [4] using XFEM, whereas Khoei et al. [35] employed a remeshing technique. Other examples of crack propagation based on stress intensity factors can be found in [36] as well as the comparison between different approaches in [3]. There are also several papers that study crack propagation based on the concept of material forces, see e.g. the discussion on computational aspects in [37] or the discussion on different propagation strategies in [38]. Furthermore, crack propagation in combination with plasticity and damage in the bulk material has been studied by many authors, using propagation models based on the stress [6, 39] or the plastic strain [8] around the crack tip.

Regardless of the propagation model chosen, there are a number of issues that will require special consideration. First, we note that the strong gradients (or singularities in elastic materials) around the crack tip will most likely cause accuracy problems if not accounted for in a proper way. In particular, evaluation of material forces can be sensitive to the mesh resolution around the crack tip. The author's opinion is that branch enrichment around crack tips (or other approaches yielding similar convergence improvements) is necessary to obtain acceptable accuracy for the material force.

Second, propagation models based on state variables (e.g. plastic strain) often require nonlocal averaging of the state variable under consideration. Since nonlocal averaging in a strongly varying field is sensitive to simulation parameters, the mesh resolution must be sufficient and the size of the averaging region must be carefully chosen with respect to the length scale over which the gradient varies.

Third, we note that the detection of crack propagation and the determination of a propagation direction need to be supplemented by the determination of the crack increment length, whereby several options are available. One option is to solve for the increment length as an additional unknown, leading to complex modeling and implementation. Another option is to employ a pure semi-explicit time integration, where cracks are propagated a fixed (predefined) distance at the end of each time step. This approach works well and is easy to implement, but it may require very small time steps and increments to obtain converged results. An alternative, which is used in the present work, is to use semi-explicit time integration for crack propagation, but to recompute the time steps until no more crack propagation occurs in the time step. This approach allows significantly larger time steps at the cost of a small complexity increase compared to a pure semi-explicit approach.

In the numerical examples presented in this thesis, propagation of XFEM cracks is modeled using the concept of material forces. Branch enrichment is used in elements containing crack tips in order to make the material force evaluation sufficiently insensitive to the radius used in the domain integral evaluation and the mesh size. We note, however, that the framework developed here is not restricted to a particular choice of crack propagation model. The crack propagation model based on material forces can easily be

replaced by a criterion based on e.g. plastic deformation around the crack tip.

4 Computational homogenization

4.1 Preliminaries

Simulating the effect of microcracks by using a mesh that is fine enough to resolve the microstructure everywhere in the domain will in most cases lead to unacceptable computational costs. A possible remedy, which reduces the computational effort without giving up the possibility to model microscale features explicitly, is to apply computational homogenization [40, 41]. The key ingredient in this strategy is the solution of a boundary value problem on a Statistical Volume Element (SVE)[1], followed by homogenization of the computed response in order to obtain the effective stress and stiffness of the microstructure. In the present work, we adopt the standard approach of first order homogenization, whereby the SVE must be sufficiently large to be representative of the microstructure, yet sufficiently small to justify the scale separation assumption.

Regarding the choice of boundary conditions (BCs) on the SVE, we remark that the boundary conditions as well as the treatment of strain localization in the SVE have a large influence on the accuracy of the method. In particular, we emphasize that the conventional BCs (Dirichlet, Neumann and strong periodic) are inaccurate if cracks intersect the SVE boundary. Dirichlet BCs suppress crack opening on the SVE boundary leading to overstiff predictions, while Neumann BCs may predict zero stiffness if cracks intersect the SVE boundary in certain ways. Strong periodic BCs can be effective, but result in overstiff predictions if cracks on the SVE boundary are not aligned with the periodicity directions. Hence, problematic overstiffening effects due to artificial crack closure on the boundary exist for both Dirichlet BCs [39, 14] and strong periodic BCs [13]. A possible remedy to the problems associated with conventional BCs is to use weakly periodic BCs as proposed by Larsson et al. [43] and later used in [44]. By enforcing periodic boundary conditions in a weak sense on the SVE, this approach allows more freedom to adapt the boundary conditions to the problem at hand as described in Section 4.3.

The problems associated with conventional BCs are even more pronounced if damage progression and localization occurs in the SVE. In particular, the SVE loses its representative character at the onset of localization in the material. Hence, localization in the SVE requires proper treatment, cf. Coenen et al. [42, 15] or Belytschko et al.[14].

In this thesis, we restrict ourselves to crack propagation in the SVE *prior* to localization and leave the proper treatment of localization in the SVE as future work. We note, however, that accurate modeling of damage progression in the SVE prior to localization is a prerequisite for accurate modeling of localization. Hence, the construction of proper boundary conditions on the SVE in the presence of propagating cracks is studied in detail in the present work.

[1] In the literature, different authors denote a sample of the microstructure *Representative Volume Element (RVE)*, *Statistical Volume Element (SVE)* or *Microstructural Volume Element*[42]. We choose to use the term *Statistical Volume Element (SVE)*.

Paper A contains a derivation of the finite element formulation for the problem under consideration using computational homogenization and weakly periodic boundary conditions. As a supplement to the developments in Paper A, we discuss the macroscale problem in Section 4.2, followed by a discussion on the microscale problem in Section 4.3.

4.2 Macroscale problem

We wish to homogenize the response of an SVE where propagating microcracks are modeled explicitly. To this end, recall the variational format given by Equation (3.2) as

$$\int_\Omega \boldsymbol{\sigma} : [\delta \boldsymbol{u} \otimes \boldsymbol{\nabla}] \, \mathrm{d}\Omega - \int_{\Gamma^+_{int}} \boldsymbol{t} \cdot [\![\delta \boldsymbol{u}]\!] \, \mathrm{d}\Gamma = \int_{\Gamma_{ext,N}} \hat{\boldsymbol{t}} \cdot \delta \boldsymbol{u} \, \mathrm{d}\Gamma \; \forall \delta \boldsymbol{u} \in \mathbb{U}^0.$$

Consider the domain decomposition $\Omega = \cup_j \, \Omega^j_\square$ and the corresponding internal boundary decomposition $\Gamma^+_{int} = \cup_j \, \Gamma^{+,j}_{\square,int}$, where $\Gamma^{+,j}_{\square,int} = \Gamma^+_{int} \cap \Omega^j_\square$ is the part of Γ^+_{int} located inside $\Omega_\square$. By inserting these decompositions in Equation (3.2), we may write

$$\int_\Omega \boldsymbol{\sigma} : [\delta \boldsymbol{u} \otimes \boldsymbol{\nabla}] \, \mathrm{d}\Omega = \sum_j \int_{\Omega^j_\square} \boldsymbol{\sigma} : [\delta \boldsymbol{u} \otimes \boldsymbol{\nabla}] \, \mathrm{d}\Omega, \tag{4.1}$$

$$\int_{\Gamma^+_{int}} \boldsymbol{t} \cdot [\![\delta \boldsymbol{u}]\!] \, \mathrm{d}\Gamma = \sum_j \int_{\Gamma^{+,j}_{\square,int}} \boldsymbol{t} \cdot [\![\delta \boldsymbol{u}]\!] \, \mathrm{d}\Gamma. \tag{4.2}$$

Inserting Equations (4.1) and (4.2) in Equation (3.2) gives

$$\sum_j \left(\int_{\Omega^j_\square} \boldsymbol{\sigma} : [\delta \boldsymbol{u} \otimes \boldsymbol{\nabla}] \, \mathrm{d}\Omega - \int_{\Gamma^{+,j}_{\square,int}} \boldsymbol{t} \cdot [\![\delta \boldsymbol{u}]\!] \, \mathrm{d}\Gamma \right) = \int_{\Gamma_{ext,N}} \hat{\boldsymbol{t}} \cdot \delta \boldsymbol{u} \, \mathrm{d}\Gamma \; \forall \delta \boldsymbol{u} \in \mathbb{U}^0. \tag{4.3}$$

Setting $\Omega_\square(\boldsymbol{x}) = \Omega^j_\square$ when $\boldsymbol{x} \in \Omega^j_\square$, so that $|\Omega_\square| = |\Omega^j_\square| = \int_{\Omega^j_\square} \mathrm{d}V$, we note that

$$\begin{aligned} \int_{\Omega^j_\square} \boldsymbol{\sigma} : [\delta \boldsymbol{u} \otimes \boldsymbol{\nabla}] \, \mathrm{d}\Omega &= \frac{1}{|\Omega^j_\square|} \int_{\Omega^j_\square} \mathrm{d}V \int_{\Omega^j_\square} \boldsymbol{\sigma} : [\delta \boldsymbol{u} \otimes \boldsymbol{\nabla}] \, \mathrm{d}\Omega = \\ &= \int_{\Omega^j_\square} \frac{1}{|\Omega^j_\square|} \int_{\Omega^j_\square} \boldsymbol{\sigma} : [\delta \boldsymbol{u} \otimes \boldsymbol{\nabla}] \, \mathrm{d}\Omega \, \mathrm{d}V, \end{aligned} \tag{4.4}$$

and, in the same way,

$$\begin{aligned} \int_{\Gamma^{+,j}_{\square,int}} \boldsymbol{t} \cdot [\![\delta \boldsymbol{u}]\!] \, \mathrm{d}\Gamma &= \frac{1}{|\Omega^j_\square|} \int_{\Omega^j_\square} \mathrm{d}V \int_{\Gamma^{+,j}_{\square,int}} \boldsymbol{t} \cdot [\![\delta \boldsymbol{u}]\!] \, \mathrm{d}\Gamma = \\ &= \int_{\Omega^j_\square} \frac{1}{|\Omega^j_\square|} \int_{\Gamma^{+,j}_{\square,int}} \boldsymbol{t} \cdot [\![\delta \boldsymbol{u}]\!] \, \mathrm{d}\Gamma \, \mathrm{d}V. \end{aligned} \tag{4.5}$$

Inserting Equations (4.4) and (4.5) in Equation (4.3) gives

$$\sum_j \left[\int_{\Omega^j_\square} \frac{1}{|\Omega^j_\square|} \left(\int_{\Omega^j_\square} \boldsymbol{\sigma} : [\delta \boldsymbol{u} \otimes \boldsymbol{\nabla}] \, \mathrm{d}\Omega - \int_{\Gamma^{+,j}_{\square,int}} \boldsymbol{t} \cdot [\![\delta \boldsymbol{u}]\!] \, \mathrm{d}\Gamma \right) \mathrm{d}V \right] = \int_{\Gamma_{ext,N}} \hat{\boldsymbol{t}} \cdot \delta \boldsymbol{u} \, \mathrm{d}\Gamma. \tag{4.6}$$

To rewrite the above sum as an integral, we consider the homogeneous macroscale domain $\bar{\Omega} = \Omega \cup \Gamma_{int}$ and express Equation (4.6) as

$$\int_{\bar{\Omega}} \frac{1}{|\Omega_\square|} \left(\int_{\Omega_\square} \boldsymbol{\sigma} : [\delta \boldsymbol{u} \otimes \boldsymbol{\nabla}] \, \mathrm{d}\Omega - \int_{\Gamma^+_{\square,int}} \boldsymbol{t} \cdot [\![\delta \boldsymbol{u}]\!] \, \mathrm{d}\Gamma \right) \mathrm{d}V = \int_{\Gamma_{ext,N}} \hat{\boldsymbol{t}} \cdot \delta \boldsymbol{u} \, \mathrm{d}\Gamma. \tag{4.7}$$

We note that Equation (4.7) is exact for perfectly matching, nonoverlapping SVEs, while smoothing results from choosing overlapping SVEs. In standard fashion, we now split the solution field according to $\boldsymbol{u} = \boldsymbol{u}^M + \boldsymbol{u}^s$ and employ first order homogenization by setting $\boldsymbol{u}^M = \bar{\boldsymbol{u}} + (\bar{\boldsymbol{u}} \otimes \boldsymbol{\nabla}) \cdot [\boldsymbol{x} - \bar{\boldsymbol{x}}]$. Since $\boldsymbol{u} \otimes \boldsymbol{\nabla} = \bar{\boldsymbol{u}} \otimes \boldsymbol{\nabla} + \boldsymbol{u}^s \otimes \boldsymbol{\nabla}$, elaborating on the terms in Equation (4.7) gives

$$\begin{aligned} \boldsymbol{\sigma} : [\delta \boldsymbol{u} \otimes \boldsymbol{\nabla}] &= \boldsymbol{\sigma} : [\delta \bar{\boldsymbol{u}} \otimes \boldsymbol{\nabla}] + \boldsymbol{\sigma} : [\delta \boldsymbol{u}^s \otimes \boldsymbol{\nabla}] \,, \\ \boldsymbol{t} \cdot [\![\delta \boldsymbol{u}]\!] &= \boldsymbol{t} \cdot \underbrace{[\![\delta \bar{\boldsymbol{u}}]\!]}_{=0} + \boldsymbol{t} \cdot \underbrace{[\![(\delta \bar{\boldsymbol{u}} \otimes \boldsymbol{\nabla}) \cdot (\boldsymbol{x} - \bar{\boldsymbol{x}})]\!]}_{=0} + \boldsymbol{t} \cdot [\![\delta \boldsymbol{u}^s]\!] = \boldsymbol{t} \cdot [\![\delta \boldsymbol{u}^s]\!]. \end{aligned}$$

Inserting in Equation (4.7) yields

$$\begin{aligned} \int_{\bar{\Omega}} \frac{1}{|\Omega_\square|} \left(\int_{\Omega_\square} \boldsymbol{\sigma} : [\delta \bar{\boldsymbol{u}} \otimes \boldsymbol{\nabla}] \, \mathrm{d}\Omega + \int_{\Omega_\square} \boldsymbol{\sigma} : [\delta \boldsymbol{u}^s \otimes \boldsymbol{\nabla}] \, \mathrm{d}\Omega - \int_{\Gamma^+_{\square,int}} \boldsymbol{t} \cdot [\![\delta \boldsymbol{u}^s]\!] \, \mathrm{d}\Gamma \right) \mathrm{d}V = \\ = \int_{\Gamma_{ext,N}} \hat{\boldsymbol{t}} \cdot \delta \boldsymbol{u} \, \mathrm{d}\Gamma. \end{aligned} \tag{4.8}$$

Assuming the pertinent microscale problem to satisfy[2]

$$a_\square \left(\boldsymbol{u}, \delta \boldsymbol{u}^s \right) \overset{\text{def}}{=} \frac{1}{|\Omega_\square|} \left[\int_{\Omega_\square} \boldsymbol{\sigma} : [\delta \boldsymbol{u}^s \otimes \boldsymbol{\nabla}] \, \mathrm{d}\Omega - \int_{\Gamma^+_{\square,int}} \boldsymbol{t} \cdot [\![\delta \boldsymbol{u}^s]\!] \, \mathrm{d}\Gamma \right] = 0, \tag{4.9}$$

and exploiting that $\delta \bar{\boldsymbol{u}} \otimes \boldsymbol{\nabla}$ is constant within $\Omega_\square$, we have

$$\int_{\bar{\Omega}} \underbrace{\left(\frac{1}{|\Omega_\square|} \int_{\Omega_\square} \boldsymbol{\sigma} \, \mathrm{d}\Omega \right)}_{\overset{\text{def}}{=} \bar{\boldsymbol{\sigma}}} : [\delta \bar{\boldsymbol{u}} \otimes \boldsymbol{\nabla}] \, \mathrm{d}\Omega = \int_{\Gamma_{ext,N}} \hat{\boldsymbol{t}} \cdot \delta \boldsymbol{u} \, \mathrm{d}\Gamma,$$

which gives us the effective stress as

$$\bar{\boldsymbol{\sigma}} \overset{\text{def}}{=} \frac{1}{|\Omega_\square|} \int_{\Omega_\square} \boldsymbol{\sigma} \, \mathrm{d}\Omega. \tag{4.10}$$

Finally, neglecting inhomogeneity on the external boundary, we assume

$$\int_{\Gamma_{ext,N}} \hat{\boldsymbol{t}} \cdot \delta \boldsymbol{u} \, \mathrm{d}\Gamma \approx \int_{\Gamma_{ext,N}} \hat{\boldsymbol{t}} \cdot \delta \bar{\boldsymbol{u}} \, \mathrm{d}\Gamma. \tag{4.11}$$

[2]We show below that $a_\square \left(\boldsymbol{u}, \delta \boldsymbol{u}^s \right)$ is indeed zero for the weakly periodic boundary conditions considered here.

Hence, the macroscale problem is solved by finding $\bar{\boldsymbol{u}} \in \bar{\mathbb{U}}$ such that

$$\begin{aligned}\int_{\bar{\Omega}} \bar{\boldsymbol{\sigma}} : [\delta\bar{\boldsymbol{u}} \otimes \boldsymbol{\nabla}] \,\mathrm{d}\Omega = \int_{\Gamma_{ext,N}} \hat{\boldsymbol{t}} \cdot \delta\bar{\boldsymbol{u}} \,\mathrm{d}\Gamma \;\forall \delta\bar{\boldsymbol{u}} \in \bar{\mathbb{U}}^0,\\ \bar{\mathbb{U}} = \left\{ \boldsymbol{v} \in \left[\mathbb{H}^1\big(\bar{\Omega}\big)\right]^d,\; \boldsymbol{v} = \hat{\boldsymbol{u}} \text{ on } \Gamma_{ext,D} \right\},\\ \bar{\mathbb{U}}^0 = \left\{ \boldsymbol{v} \in \left[\mathbb{H}^1\big(\bar{\Omega}\big)\right]^d,\; \boldsymbol{v} = \boldsymbol{0} \text{ on } \Gamma_{ext,D} \right\}.\end{aligned} \tag{4.12}$$

4.3 Microscale problem

4.3.1 Weakly periodic boundary conditions

Variational formulation

Equation (4.10) gives an expression for the effective stress that allows the homogenized response of an SVE to be computed, provided that the SVE problem has been solved. Here, we aim to solve the SVE problem by imposing periodic boundary conditions on the SVE in a weak sense. To this end, we first divide the SVE boundary into an image part $\Gamma_\square^+$ and a mirror part $\Gamma_\square^-$ as shown in Figure 4.1. Furthermore, we introduce a mapping $\boldsymbol{\varphi}_{per} : \Gamma_\square^+ \to \Gamma_\square^-$ such that $\boldsymbol{x}^- = \boldsymbol{\varphi}_{per}(\boldsymbol{x}^+)$ and define

$$[\![\boldsymbol{u}(\boldsymbol{x}^+)]\!]_\square \overset{\text{def}}{=} \boldsymbol{u}(\boldsymbol{x}^+) - \boldsymbol{u}(\boldsymbol{x}^-) = \boldsymbol{u}(\boldsymbol{x}^+) - \boldsymbol{u}(\boldsymbol{\varphi}_{per}(\boldsymbol{x}^+)).$$

Weak periodicity is then obtained by requiring $[\![\boldsymbol{u}]\!]_\square = \bar{\boldsymbol{\epsilon}} \cdot [\![\boldsymbol{x} - \bar{\boldsymbol{x}}]\!]_\square$ to hold weakly instead of pointwise to get the following SVE problem: Find $\boldsymbol{u} \in \mathbb{U}_\square$ and $\boldsymbol{t}_\lambda \in \mathbb{T}_\square$ such that

$$\begin{aligned} a_\square(\boldsymbol{u}, \delta\boldsymbol{u}) - d_\square(\boldsymbol{t}_\lambda, \delta\boldsymbol{u}) = 0 \;\forall \delta\boldsymbol{u} \in \mathbb{U}_\square,\\ -d_\square(\delta\boldsymbol{t}_\lambda, \boldsymbol{u}) = -d_\square(\delta\boldsymbol{t}_\lambda, \bar{\boldsymbol{\epsilon}} \cdot [\boldsymbol{x} - \bar{\boldsymbol{x}}]) \;\forall \delta\boldsymbol{t}_\lambda \in \mathbb{T}_\square, \end{aligned} \tag{4.13}$$

$$\mathbb{U}_\square = \{\boldsymbol{v} : \boldsymbol{v} \in \left[\mathbb{H}^1(\Omega_\square)\right]^d,\; \int_{\Gamma_\square} \boldsymbol{v} \,\mathrm{d}\Gamma = \boldsymbol{0}\}, \tag{4.14}$$

$$\mathbb{T}_\square = \{\boldsymbol{v} : \boldsymbol{v} \in \left[\mathbb{L}_2\big(\Gamma_\square^+\big)\right]^d\}, \tag{4.15}$$

where we introduced the expressions

$$a_\square(\boldsymbol{u}, \delta\boldsymbol{u}) \overset{\text{def}}{=} \frac{1}{|\Omega_\square|} \left[\int_{\Omega_\square} \boldsymbol{\sigma} : \boldsymbol{\epsilon}[\delta\boldsymbol{u}] \,\mathrm{d}\Omega - \int_{\Gamma_{\square,int}^+} \boldsymbol{t} \cdot [\![\delta\boldsymbol{u}]\!] \,\mathrm{d}\Gamma \right], \tag{4.16}$$

$$d_\square(\boldsymbol{t}_\lambda, \delta\boldsymbol{u}) \overset{\text{def}}{=} \frac{1}{|\Omega_\square|} \int_{\Gamma_\square^+} \boldsymbol{t}_\lambda \cdot [\![\delta\boldsymbol{u}]\!]_\square \,\mathrm{d}\Gamma \tag{4.17}$$

and $\mathbb{L}_2\big(\Gamma_\square^+\big)$ denotes the space of square integrable functions on $\Gamma_\square^+$.

Now recall the discussion in Section 4.2, where it was claimed that

$$a_\square(\boldsymbol{u}, \delta\boldsymbol{u}^s) = \int_{\Omega_\square} \boldsymbol{\sigma} : [\delta\boldsymbol{u}^s \otimes \boldsymbol{\nabla}] \,\mathrm{d}\Omega - \int_{\Gamma_{\square,int}^+} \boldsymbol{t} \cdot [\![\delta\boldsymbol{u}^s]\!] \,\mathrm{d}\Gamma = 0. \tag{4.18}$$

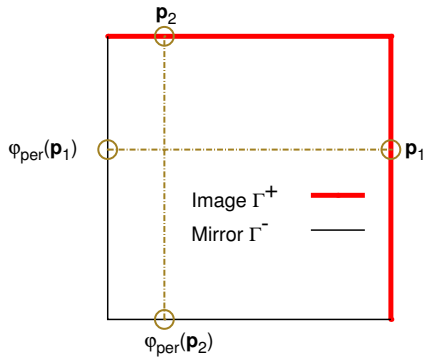

Figure 4.1: *The SVE boundary* $\Gamma_\square$ *is split into an image part* $\Gamma_\square^+$ *and a mirror part* $\Gamma_\square^-$. *The mapping* $\boldsymbol{\varphi}_{per}$ *between associated points on* $\Gamma_\square^+$ *and* $\Gamma_\square^-$ *is also indicated.*

To show this identity, note that from Equation (4.13), we have $a_\square(\boldsymbol{u}, \delta\boldsymbol{u}^s) = d_\square(\boldsymbol{t}_\lambda, \delta\boldsymbol{u}^s)$. Using the relation

$$\delta\boldsymbol{u}^s = \delta\boldsymbol{u} - \delta\bar{\boldsymbol{u}} - (\delta\bar{\boldsymbol{u}} \otimes \boldsymbol{\nabla}) \cdot [\boldsymbol{x} - \bar{\boldsymbol{x}}], \tag{4.19}$$

we have

$$d_\square(\boldsymbol{t}_\lambda, \delta\boldsymbol{u}^s) = d_\square(\boldsymbol{t}_\lambda, \delta\boldsymbol{u}) - d_\square(\boldsymbol{t}_\lambda, \delta\bar{\boldsymbol{u}}) - d_\square(\boldsymbol{t}_\lambda, (\delta\bar{\boldsymbol{u}} \otimes \boldsymbol{\nabla}) \cdot [\boldsymbol{x} - \bar{\boldsymbol{x}}]). \tag{4.20}$$

Since $d_\square(\boldsymbol{t}_\lambda, \delta\bar{\boldsymbol{u}}) = 0$ for a constant $\delta\bar{\boldsymbol{u}}$, and due to the fact that the solution $\boldsymbol{t}_\lambda \in \mathbb{T}_\square$, we conclude from Equations (4.19) and (4.20) that

$$a_\square(\boldsymbol{u}, \delta\boldsymbol{u}^s) = d_\square(\boldsymbol{t}_\lambda, \delta\boldsymbol{u}) - d_\square(\boldsymbol{t}_\lambda, [\delta\bar{\boldsymbol{u}} \otimes \boldsymbol{\nabla}] \cdot [\boldsymbol{x} - \bar{\boldsymbol{x}}]) = 0. \tag{4.21}$$

To see the relation to the so-called Hill-Mandel condition, we note that inserting this relation in Equation (4.8) gives

$$a_\square(\boldsymbol{u}, \delta\boldsymbol{u}) = \frac{1}{|\Omega_\square|} \int_{\Omega_\square} \boldsymbol{\sigma} : [\delta\bar{\boldsymbol{u}} \otimes \boldsymbol{\nabla}] \, \mathrm{d}\Omega = \bar{\boldsymbol{\sigma}} : [\delta\bar{\boldsymbol{u}} \otimes \boldsymbol{\nabla}] = \bar{\boldsymbol{\sigma}} : \delta\bar{\boldsymbol{\epsilon}},$$

i.e. the virtual work on the macroscale is equal to the average virtual work on the microscale. See [43] for further discussion.

Traction discretization

Solving the finite element problem associated to Equation (4.13) requires construction of $\mathbb{U}_\square^h$ and $\mathbb{T}_\square^h$. A conventional FE mesh will be used to construct $\mathbb{U}_\square^h$, whereas $\mathbb{T}_\square^h$ can be constructed using a global polynomial basis [44] or by means of a traction mesh on the SVE boundary [43]. Choosing the latter option, we construct a (one-dimensional) traction mesh on $\Gamma_\square^+$, defined by traction nodes and two-node traction elements. The traction is then assumed to be piecewise constant or linear on each traction element.

To construct a traction mesh, we start from the approach in [43], where the first step is to project all (displacement) nodes on the image boundary as well as the mirror boundary onto the image boundary, as shown in Figure 4.2. Points where cracks or grain boundaries intersect the boundary are projected in the same way. Next, points that are closer to each other than a given tolerance are merged, in order to prevent that traction elements become too small. Performing these steps results in a dense traction mesh that can be used as it is, or coarsened as indicated to the right in Figure 4.2.

In the present work, we are interested in a particular choice for the traction mesh. We consider a piecewise constant traction approximation, that is coarsened so much that only traction nodes at SVE corners and crack-boundary intersections are retained as shown in Figure 4.3. This approximation often performs very well, as shown in Paper A and Paper B.

Here, we will supplement the discussion in the appended papers with some additional remarks regarding the stability properties of the discretization. Since a mixed formulation is employed, the LBB (inf-sup) condition needs to be fulfilled. Recalling that we consider piecewise linear and piecewise constant traction approximations, we first remark that piecewise linear traction approximations generated using the strategy above fulfill the LBB condition [43]. (Note, however, the discussion on additional periodicity constraints for the traction in [43].) The situation is less straightforward for a piecewise constant traction approximation. On the one hand, it is known that a piecewise constant traction approximation on each linear displacement element fails to fulfill the LBB condition, cf. El-Abbasi and Bathe [45] in the context of contact. On the other hand, Neumann boundary conditions, which correspond the coarsest possible piecewise constant traction approximation, are stable. For piecewise constant traction approximations that are in between these two extremes (i.e. for a "moderately dense" traction mesh), it is nontrivial to assess whether the LBB condition is fulfilled or not. In the present work, a traction approximation that is piecewise constant between crack-boundary intersections and SVE corners, as shown in Figure 4.3, has shown promising results. Therefore, it is interesting to investigate if this particular choice for the traction approximation fulfills the LBB condition. In Paper A, we show analytically that this particular choice of piecewise constant traction approximation indeed fulfills the LBB condition.

As a supplement to the stability proof in Paper A, we will here give a numerical example in order to illustrate the assumptions behind the proof and to provide a simple interpretation. The proof given in Paper A states that the LBB condition is fulfilled if at least one displacement node is located inside each traction element and the size of the traction elements is kept constant when refining the displacement elements. To illustrate this condition with the simplest possible example, we consider a homogeneous SVE (pure, homogeneous material without cracks or inclusions) discretized with 10×10 quadrilateral elements. The material is linear elastic with Young's modulus $E = 10$ and Poisson's ratio $\nu = 0.3$. We use weakly periodic boundary conditions to apply a uniaxial effective strain $\bar{\epsilon}_{xx} = 1$, whereby three different traction meshes are considered as shown in Figure 4.4: **Mesh A** where all displacement nodes are retained, **Mesh B** where every second displacement node is retained and **Mesh C** where every fifth displacement node is retained. We note that Mesh B and Mesh C have at least one displacement node inside each traction element, so we expect these discretizations to give stable response. However,

Mesh A does not have at least one displacement node inside each traction element, so we cannot expect Mesh A to give stable response. Solving the SVE problem with these three meshes and computing the condition number of the global stiffness matrix gives the following result:

- Mesh A gives a condition number of 10^{25},
- Mesh B gives a condition number of 10^{8},
- Mesh C gives a condition number of 10^{7}.

Mesh A results in a very high condition number that indicates numerical problems, whereas Mesh B and Mesh C lead to well conditioned matrices. The instability indicated by the high condition number obtained with Mesh A pollutes the solution for the boundary traction as shown in Figure 4.5: Mesh B and Mesh C lead to smooth boundary tractions, whereas Mesh A leads to an oscillatory solution.

With the simple example above in mind, we emphasize that the piecewise constant traction approximation is stable provided that:

1. At least one displacement node is located inside each traction element. This is a reasonable assumption for a sufficiently fine displacement mesh, provided that the traction elements are not allowed to be too small (see also the discussion on removing traction nodes that are too close in [43]).

2. The length of the traction elements must not tend to zero as the displacement elements are refined. This requirement is fulfilled in the present work, because the traction mesh is created based on the locations of cracks or grain boundaries, and these positions do not change under mesh refinement.

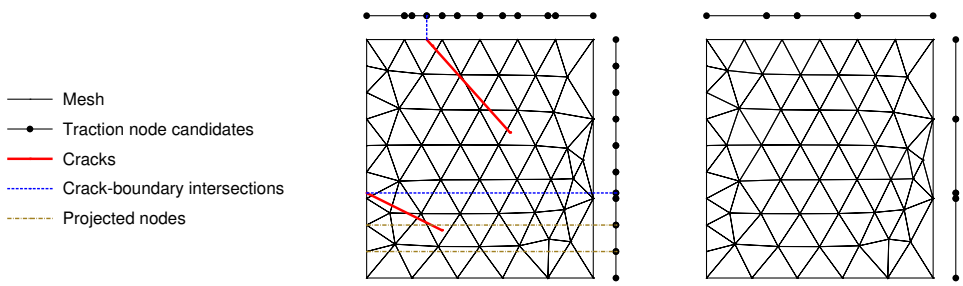

Figure 4.2: *Traction discretization: unprocessed (left) and processed (right) traction meshes. Addition of traction nodes where cracks intersect the boundary is indicated to the left.*

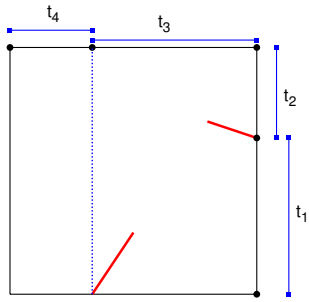

Figure 4.3: *Piecewise constant traction approximation with traction discontinuities at SVE boundaries and crack-boundary intersections.*

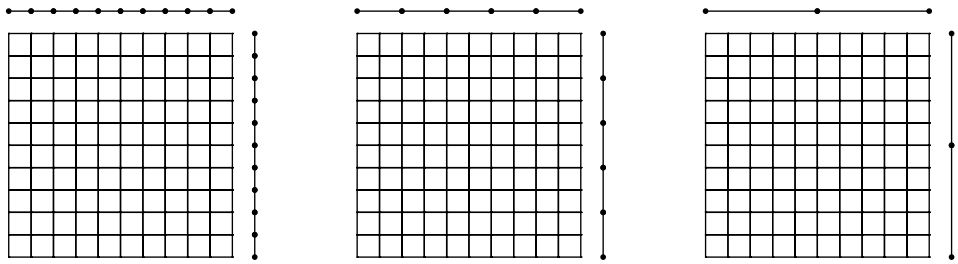

(a) *Mesh A: all displacement nodes are retained.* (b) *Mesh B: every second displacement node is retained.* (c) *Mesh C: every fifth displacement node is retained.*

Figure 4.4: *Traction meshes for illustration of the LBB condition.*

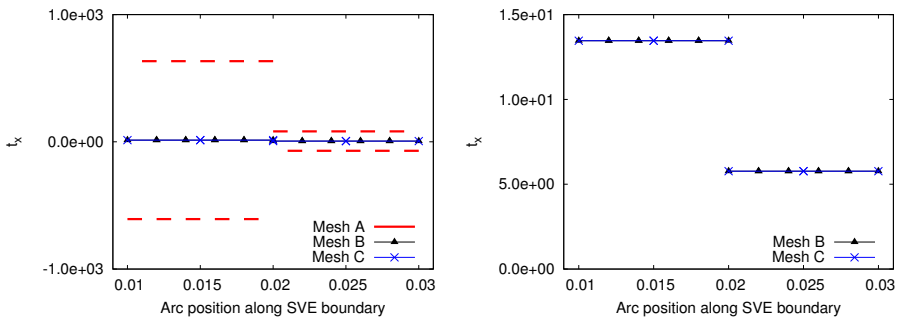

(a) *Y-axis range from* $-1.0 \cdot 10^3$ *to* $1.0 \cdot 10^3$. (b) *Y-axis range from* 0.0 *to* 15.0.

Figure 4.5: *Traction along* $\Gamma^+_\square$ *computed with different traction meshes. We display the results with a wide y-axis range (left) to show the oscillatory response obtained with Mesh A and a zoomed in plot (right) to show the smooth response obtained with Mesh B and Mesh C. We note that the densest traction discretization (Mesh A) is obviously unstable. (We also note that the traction is discontinuous across the SVE corner, since the normal of the boundary is discontinuous there.)*

4.3.2 Problems with conventional boundary conditions

As discussed previously, conventional BCs perform poorly if cracks intersect the SVE boundary. Here, a small example is given that demonstrates how the deficiencies of conventional BCs may affect the solution of the SVE problem in practice. To this end, consider the SVE shown in Figure 4.6. The side length of the SVE is 0.01 and we assume that the material is linear elastic with Young's modulus $E = 210 \cdot 10^3$ and Poisson's ratio $\nu = 0.3$. To obtain a solvable problem also when Neumann BCs are used, an elastic cohesive zone with a stiffness of $K = 1.0 \cdot 10^3$ is used in all examples. A macroscopic strain of $\bar{\epsilon}_{xx} = 0.1,\ \bar{\epsilon}_{yy} = 0.1,\ \bar{\epsilon}_{xy} = 0$ is imposed on the SVE using Dirichlet BCs, weakly periodic BCs with dense traction discretization (corresponding to strong periodic BCs), Neumann BCs and weakly periodic BCs with piecewise constant traction between crack-boundary intersections. The solution obtained with the different BCs listed above is shown in Figure 4.7. We note that Dirichlet BCs as well as strong periodic BCs enforce crack closure on the SVE boundary, leading to overstiff predictions. Neumann BCs predict very low stresses, leading to severe underprediction of the stiffness. Weakly periodic BCs with piecewise constant traction between crack-boundary intersections do not enforce artificial crack closure on the boundary, but still predict reasonable stresses in the microstructure.

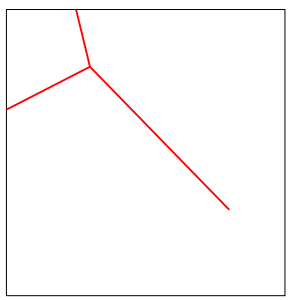

Figure 4.6: *SVE used for illustration of the problems associated to conventional BCs.*

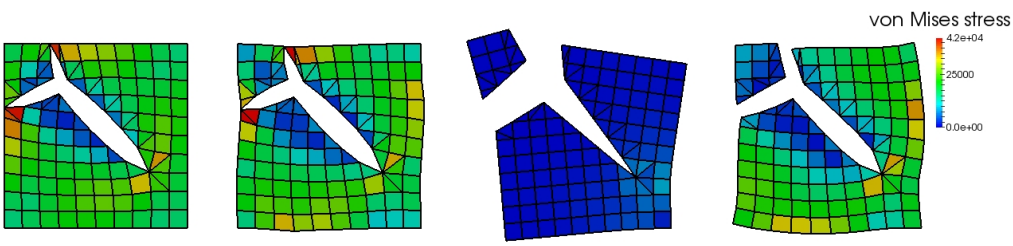

Figure 4.7: *SVE subject to a macroscopic strain of* $\bar{\epsilon}_{xx} = 0.1,\ \bar{\epsilon}_{xy} = 0.1,\ \bar{\epsilon}_{xy} = 0$. *The solution was computed by (from left to right): Dirichlet BCs, weakly periodic BCs with dense traction discretization (corresponding to strong periodic BCs), Neumann BCs and weakly periodic BCs with piecewise constant traction between crack-boundary intersections.*

5 Implementation

The model developed in the present work has been implemented in the open source software package OOFEM [46, 47] and can be downloaded from `https://github.com/erisve/oofem`. The grain structures considered in paper B were prepared using Neper [48, 49] and Phon [50]. The post-processing was done with Paraview [51] and Gnuplot [52].

6 Summary of appended papers

6.1 Paper A: Computational homogenization of microfractured continua using weakly periodic boundary conditions

Computational homogenization of an elastic material containing stationary microcracks is considered, whereby the cracks are modeled using the eXtended Finite Element Method (XFEM). Weakly periodic boundary conditions are imposed on the Statistical Volume Element (SVE), leading to a mixed variational formulation with displacements and boundary tractions as unknowns. We consider the traction approximation as a modeling choice and develop an approximation that is suitable when cracks intersect the SVE boundary. The main result is the proposition of a stable traction approximation that is piecewise constant between crack-boundary intersections. In particular, we prove analytically that the proposed approximation is stable in terms of the LBB (inf-sup) condition. The numerical examples show that the proposed traction approximation is more efficient than conventional boundary conditions (Dirichlet, Neumann, strong periodic) in terms of convergence with increasing SVE size.

6.2 Paper B: Computational homogenization of microstructures undergoing crack propagation

The model developed in Paper A is extended to handle propagating cracks. For the modeling of crack propagation, we consider i) XFEM in combination with the concept of material forces and ii) conventional cohesive zone elements. The numerical examples show that weakly periodic boundary conditions, with piecewise constant traction approximation between crack-boundary intersections, are effective also when damage progression occurs in the microstructure.

7 Conclusions and future work

The present work is concerned with computational homogenization of microstructures containing propagating cracks, whereby the effective response is determined from the response of Statistical Volume Elements (SVEs). To obtain accurate results, the choice of boundary conditions (BCs) on the SVE is critical. Choosing suitable BCs is particularly challenging in the case considered here, since conventional BCs (Neumann, Dirichlet and strong periodic) are inaccurate when cracks are present in the SVE. We remark that the problems associated with conventional BCs occur both for stationary cracks as shown in Paper A and for propagating cracks as shown in Paper B. As a remedy, we employ weakly periodic BCs with a piecewise constant traction approximation between crack-boundary intersections. This traction approximation, which can be considered as the smallest possible refinement of Neumann BCs, turns out to be more effective than conventional BCs in terms of convergence with increasing SVE size. This is a significant advantage, because a smaller SVE can be used without loss of accuracy, leading to reduced computational costs. The efficiency of the proposed approximation is demonstrated for stationary cracks in Paper A and for propagating cracks in Paper B. Furthermore, we show in Paper A that the proposed approximation fulfills the LBB (inf-sup) condition.

An interesting conclusion from the present work is that it is possible to outperform conventional BCs (including strong periodic BCs) by exploiting available geometric information about the problem at hand. The proposed approach works well for discrete cracks, where distinct crack-boundary intersections can be readily identified. If damage progression in the SVE is modeled using a (local or nonlocal) continuum damage model, additional effort is needed to create a suitable traction discretization. An interesting possibility is combine the present work with the image analysis technique used by Coenen et al. [42] in the context of rotated periodic BCs.

Regarding future work, we remark that the results presented in this thesis are restricted to upscaling of the response prior to localization. An obvious next step is to develop an FE^2-scheme to allow concurrent multiscale modeling. Furthermore, a natural extension of the present work is to address localization in the SVE leading to the evolution of a macroscopic crack. Interesting work along these lines is the percolation path aligned BCs in [42, 15, 16], the Multiscale Aggregating Discontinuities (MAD) method by Belytschko et al. [14] and the different fracture models adopted in [11, 12, 13]. An alternative approach could be to refine the macroscale mesh around the localizing SVE in order to resolve the crack on the macroscale.

We also note that the results presented in this thesis are restricted to linear elastic bulk material. An interesting extension is to consider material models that better describe the microscale behavior of metals. A suitable candidate is crystal plasticity [53, 54] in combination with tailored crack propagation models [10] and models of the grain microstructure [49].

Finally, since the present work is restricted to 2D, a natural extension is to consider 3D models. The main challenge associated with such 3D models is probably the construction of a suitable traction mesh and the implementation effort associated with propagating XFEM cracks in 3D.

References

[1] M. Jirásek. Modeling of Localized Inelastic Deformation. *Thakurova* **7**.166 (2012), 29.

[2] J. Lemaitre and H. Lippmann. *A course on damage mechanics*. Springer Berlin, 1996.

[3] P. Dumstorff and G. Meschke. Crack propagation criteria in the framework of X-FEM-based structural analyses. *International Journal for Numerical and Analytical Methods in Geomechanics* **31**.2 (Feb. 2007), 239–259.

[4] G. Zi and T. Belytschko. New crack-tip elements for XFEM and applications to cohesive cracks. *International Journal for Numerical Methods in Engineering* **57**.15 (Aug. 2003), 2221–2240.

[5] R. Larsson and M. Fagerström. A framework for fracture modelling based on the material forces concept with XFEM kinematics. *International Journal for Numerical Methods in Engineering* **62**.13 (Apr. 2005), 1763–1788.

[6] M. Fagerström and R. Larsson. Approaches to dynamic fracture modelling at finite deformations. *Journal of the Mechanics and Physics of Solids* **56**.2 (Feb. 2008), 613–639.

[7] V. P. Nguyen, O. Lloberas-Valls, M. Stroeven, and L. J. Sluys. Computational homogenization for multiscale crack modeling. Implementational and computational aspects. *International Journal for Numerical Methods in Engineering* **89**.2 (Jan. 2012), 192–226.

[8] G. N. Wells. *Discontinuous modelling of strain localisation and failure*. Delft University of Technology, 2001.

[9] P. M. A. Areias and T. Belytschko. Analysis of three-dimensional crack initiation and propagation using the extended finite element method. *International Journal for Numerical Methods in Engineering* **63** (2005), 760–788.

[10] R. Lillbacka, E. Johnson, and M. Ekh. A model for short crack propagation in polycrystalline materials. *Engineering Fracture Mechanics* **73**.2 (Jan. 2006), 223–232.

[11] V. Nguyen, M. Stroeven, and L. Sluys. Multiscale continuous and discontinuous modeling of heterogeneous materials: A review on recent developments. *Journal of Multiscale Modelling* **3**.04 (2011), 229–270.

[12] F. V. Souza and D. H. Allen. Modeling the transition of microcracks into macrocracks in heterogeneous viscoelastic media using a two-way coupled multiscale model. *International Journal of Solids and Structures* **48**.22-23 (Nov. 2011), 3160–3175.

[13] H. Talebi, M. Silani, S. P. A. Bordas, P. Kerfriden, and T. Rabczuk. A computational library for multiscale modeling of material failure. *Computational Mechanics* **53**.5 (Dec. 2013), 1047–1071.

[14] T. Belytschko, S. Loehnert, and J.-H. Song. Multiscale aggregating discontinuities: A method for circumventing loss of material stability. *International Journal for Numerical Methods in Engineering* **73**.6 (Feb. 2008), 869–894.

[15] E. W. C. Coenen, V. G. Kouznetsova, E. Bosco, and M. G. D. Geers. A multi-scale approach to bridge microscale damage and macroscale failure: a nested computational

homogenization-localization framework. *International Journal of Fracture* **178**.1-2 (Sept. 2012), 157–178.

[16] E. Bosco, V. G. Kouznetsova, E. W. C. Coenen, M. G. D. Geers, and A. Salvadori. A multiscale framework for localizing microstructures towards the onset of macroscopic discontinuity. *Computational Mechanics* **54**.2 (Feb. 2014), 299–319.

[17] T. Belytschko and T. Black. Elastic crack growth in finite elements with minimal remeshing. *International Journal for Numerical Methods in Engineering* **45**.5 (1999), 601–620.

[18] T. Fries and T Belytschko. The extended/generalized finite element method: an overview of the method and its applications. *International Journal for Numerical Methods in Engineering* **84**.3 (Aug. 2010), 253–304.

[19] T.-P. Fries and M. Baydoun. Crack propagation with the extended finite element method and a hybrid explicit-implicit crack description. *International Journal for Numerical Methods in Engineering* **89**.12 (Mar. 2012), 1527–1558.

[20] C. Daux, N. Moës, J. Dolbow, N. Sukumar, and T. Belytschko. Arbitrary branched and intersecting cracks with the extended finite element method. *International Journal for Numerical Methods in Engineering* **48**.12 (2000), 1741–1760.

[21] N. Moës, J. Dolbow, and T. Belytschko. A finite element method for crack growth without remeshing. *International Journal for Numerical Methods in Engineering* **46**.1 (1999), 131–150.

[22] T. Belytschko, N. Moës, S. Usui, and C. Parimi. Arbitrary discontinuities in finite elements. *International Journal for Numerical Methods in Engineering* **50**.4 (Feb. 2001), 993–1013.

[23] S. Loehnert. A stabilization technique for the regularization of nearly singular extended finite elements. *Computational Mechanics* **54**.2 (Mar. 2014), 523–533.

[24] J. M. Melenk and I. Babuška. The partition of unity finite element method: Basic theory and applications. *Computer Methods in Applied Mechanics and Engineering* **139**.1-4 (1996), 289–314.

[25] D. S. Dugdale. Yielding of steel sheets containing slits. *Journal of the Mechanics and Physics of Solids* **8**.2 (1960), 100–104.

[26] G. I. Barenblatt. The Mathematical Theory of Equilibrium Cracks in Brittle Fracture. *Advances in Applied Mechanics*. Advances in Applied Mechanics **7**.C (1962), 55–129.

[27] G. N. Wells and L. J. Sluys. A new method for modelling cohesive cracks using finite elements. *International Journal for Numerical Methods in Engineering* **50**.12 (Apr. 2001), 2667–2682.

[28] M. Ortiz and A. Pandolfi. Finite-deformation irreversible cohesive elements for three-dimensional crack-propagation analysis. *International Journal for Numerical Methods in Engineering* **44**.9 (1999), 1267–1282.

[29] F. Cazes, M. Coret, and A. Combescure. A two-field modified Lagrangian formulation for robust simulations of extrinsic cohesive zone models. *Computational Mechanics* **51**.6 (Aug. 2012), 865–884.

[30] E. Lorentz. A mixed interface finite element for cohesive zone models. *Computer Methods in Applied Mechanics and Engineering* **198**.2 (Dec. 2008), 302–317.

[31] P. Hansbo and P. Heintz. "Finite element modeling of cohesive cracks by Nitsche's method". *Fracture of Nano and Engineering Materials and Structures - Proceedings*

of the 16th European Conference of Fracture. Kluwer Academic Publishers, 2006, pp. 947–948.

[32] J. C. J. Schellekens and R. De Borst. On the numerical integrations of interface elements. *International Journal for Numerical Methods in Engineering* **36**.1 (1993), 43–66.

[33] P. Wriggers. *Computational Contact Mechanics*. Berlin, Heidelberg: Springer Berlin Heidelberg, 2006, pp. 1–518.

[34] M. Fagerström and R. Larsson. Theory and numerics for finite deformation fracture modelling using strong discontinuities. *International Journal for Numerical Methods in Engineering* **66**.6 (May 2006), 911–948.

[35] A. Khoei, H. Azadi, and H. Moslemi. Modeling of crack propagation via an automatic adaptive mesh refinement based on modified superconvergent patch recovery technique. *Engineering Fracture Mechanics* **75**.10 (July 2008), 2921–2945.

[36] J. Dolbow, N. Moës, and T. Belytschko. Discontinuous enrichment in finite elements with a partition of unity method. *Finite Elements in Analysis and Design* **36**.3-4 (Nov. 2000), 235–260.

[37] P. Steinmann, D. Ackermann, and F. Barth. Application of material forces to hyperelastostatic fracture mechanics. II. Computational setting. *International Journal of Solids and Structures* **38**.32-33 (Aug. 2001), 5509–5526.

[38] J. Brouzoulis, F. Larsson, and K. Runesson. Strategies for planar crack propagation based on the concept of material forces. *Computational Mechanics* **47**.3 (Oct. 2010), 295–304.

[39] T. Hettich, A. Hund, and E. Ramm. Modeling of failure in composites by X-FEM and level sets within a multiscale framework. *Computer Methods in Applied Mechanics and Engineering* **197**.5 (Jan. 2008), 414–424.

[40] M. Geers, V. Kouznetsova, and W. Brekelmans. Multi-scale computational homogenization: Trends and challenges. *Journal of Computational and Applied Mathematics* **234**.7 (Aug. 2010), 2175–2182.

[41] T. Zohdi and P. Wriggers. A model for simulating the deterioration of structural-scale material responses of microheterogeneous solids. *Computer Methods in Applied Mechanics and Engineering* **190**.22-23 (Feb. 2001), 2803–2823.

[42] E. Coenen, V. Kouznetsova, and M. Geers. Novel boundary conditions for strain localization analyses in microstructural volume elements. *International Journal for Numerical Methods in Engineering* **90**.1 (Apr. 2012), 1–21.

[43] F. Larsson, K. Runesson, S. Saroukhani, and R. Vafadari. Computational homogenization based on a weak format of micro-periodicity for RVE-problems. *Computer Methods in Applied Mechanics and Engineering* **200**.1-4 (Jan. 2011), 11–26.

[44] C. Sandstom, F. Larsson, and K. Runesson. Weakly periodic boundary conditions for the homogenization of flow in porous media. *Advanced Modeling and Simulation in Engineering Sciences* **1**.1 (2014), 12.

[45] N. El-Abbasi and K.-J. Bathe. Stability and patch test performance of contact discretizations and a new solution algorithm. *Computers & Structures* **79**.16 (June 2001), 1473–1486.

[46] B Patzák and Z Bittnar. Design of object oriented finite element code. *Advances in Engineering Software* **32**.10-11 (Oct. 2001), 759–767.

[47] B. Patzák. *OOFEM project home page: www.oofem.org*. 2000.
[48] R. Quey. *Neper project home page*.
[49] R. Quey, P. Dawson, and F. Barbe. Large-scale 3D random polycrystals for the finite element method: Generation, meshing and remeshing. *Computer Methods in Applied Mechanics and Engineering* **200**.17-20 (Apr. 2011), 1729–1745.
[50] K. Carlsson. *Phon project home page*.
[51] Paraview. *Paraview web page*.
[52] Gnuplot. *Gnuplot web page*.
[53] M. Ekh, R. Lillbacka, and K. Runesson. A model framework for anisotropic damage coupled to crystal (visco)plasticity. *International Journal of Plasticity* **20**.12 (Dec. 2004), 2143–2159.
[54] S. Bargmann, B. Svendsen, and M. Ekh. An extended crystal plasticity model for latent hardening in polycrystals. *Computational Mechanics* **48**.6 (June 2011), 631–645.